WATER RESOURCES RESEARCH, VOL. 26, NO. 12, PAGES 2865–2880, DECEMBER 1990

A Triangular Finite Volume Approach With High-Resolution Upwind Terms for the Solution of Groundwater Transport Equations

MARIO PUTTI AND WILLIAM W.-G. YEH

Department of Civil Engineering, University of California, Los Angeles

WILLIAM A. MULDER[1]

Department of Mathematics, University of California, Los Angeles

A finite volume approach is developed for the solution of the contaminant transport equation in groundwater. By defining a triangular control volume over which the dependent variable of the governing equation is averaged, the scheme combines the flexibility in handling complex geometries intrinsic to finite element methods with the simplicity of finite difference techniques. High-resolution upwind schemes are employed for the discretization of the advective terms. The technique is based on the concept of "monotone interpolation" to ensure the monotonicity preserving property of the scheme, and on the exact solution of local Riemann problems at the interface between neighboring control volumes. In this way, numerical oscillations are completely avoided for a full range of cell Peclet numbers. Together with the discretization of the dispersive fluxes, an approximation is obtained that is locally first order, but globally of second-order accuracy. As compared to usual upwind schemes, much smaller amounts of numerical viscosity are introduced when sharp concentration fronts occur. A number of numerical tests show good agreement with analytical solutions. A hypothetical problem involving nonequilibrium reaction terms is solved to illustrate the applicability and robustness of the proposed formulation for solving the groundwater transport equations.

INTRODUCTION

Finite volume techniques have been used for a long time [*Peyret and Taylor*, 1983]. In the water resources community, however, finite difference and especially finite element methods are often preferred. The latter are more widely used in the solution to the groundwater transport equations because of their ability to describe geometrically complex domains.

When the transport is advection dominated, sharp concentration fronts are usually present. Special methods are then required in the attempt to avoid spurious oscillations and to minimize the artificial viscosity introduced, which considerably affects the resolution of the sharp front. Lagrangian techniques (method of characteristics) have been used for the discretization of advective fluxes in conjunction with standard finite difference or finite element methods for the approximation of the dispersive terms [*Neuman*, 1981, 1984; *Farmer*, 1985]. These formulations achieve high-order accuracy at the expense of high computational costs, especially in more than one space dimension.

Alternatively, upwind schemes have been extensively used in finite difference and finite element methods [*Richtmeyer and Morton*, 1967; *Zienkiewicz*, 1986]. A simple way to incorporate upwind terms in finite element techniques is described by *Sun and Yeh* [1983] for the solution of the two-dimensional groundwater contamination problem. It is based on the definition of a subdomain, incorporating parts of the elements converging to a node, over which upstream weights can easily be added. The formulation, however, requires the empirical evaluation of a parameter in order to follow the changing characteristics of the transport equation. Furthermore, it is only first-order accurate, and therefore may introduce large amounts of artificial viscosity.

To overcome this problem, schemes have been developed that are globally high-order accurate and nonoscillatory [*Roe*, 1986]. This started with MUSCL (monotone upwind schemes for conservation laws) by *van Leer* [1977*a*, *b*], which provides a higher-order extension of *Godunov*'s [1959] scheme. The basic idea can be outlined, in the one-dimensional case, as follows. First, the dependent variable is represented as a volume average in a control volume or cell. Its rate of change is determined by the fluxes across the two cell interfaces. The flux at an interface is obtained from the left and right volume averaged states by solving the local physical problem, the so-called Riemann problem, exactly. This leads to a first-order scheme. Note that, in solving the Riemann problem, the variables are assumed to be piecewise constant. Higher-order extensions can be obtained by assuming the variables in each cell to be piecewise linear, quadratic, etc. Second-order accuracy is then achieved with the determination of the linear distribution of the dependent variable in the control volumes. This is calculated by interpolation from neighboring cells. The crucial step is to do this in the following monotone way: in determining the linear distribution, no overshoots or undershoots with respect to neighboring cell averages should be created. Near discontinuities, this requirement results in slopes that are smaller than those obtained by usual interpolation. This procedure is normally referred to as "limiting." Once the piecewise linear distributions are determined, the fluxes are obtained from the solution of the local Riemann problem at the cell interfaces. The procedure results in spatial second-order accuracy on all points other

[1]Now at Koninklijke/Shell Exploratie en Produktie Laboratorium, Rijswijk, The Netherlands.

Paper number 90WR01791.
0043-1397/90/90WR-01791$05.00

than where limiting occurs, in which case the scheme becomes first-order accurate.

Harten [1983] constructed a second-order accurate TVD (total variation diminishing) upwind scheme in which an extra antidiffusive term is added to minimize artificial viscosity. The TVD property is generally a more relaxed version of the monotonocity preserving property, but still insures that the scheme does not produce nonphysical oscillations. For linear fluxes, this approach coincides with van Leer's scheme. Operational unifications of high-resolution upwind techniques have been presented by *Chakravarthy and Osher* [1985] and by *van Leer* [1985]. Extensions of this family of schemes to two space dimensions are usually based on the solution of the Riemann problems along near-orthogonal directions, using quadrilateral control volumes. It becomes difficult to describe complex geometries.

Chakravarthy and Osher [1985] introduced a procedure for the extension of such schemes to triangular elements. This finite volume approach is used and extended in the present research and is applied to the solution of the general transport equations in groundwater. The formulation is very attractive for this problem as an alternative to finite difference and finite element methods [*Putti*, 1989]. It combines the flexibility of finite elements in describing complicated geometries with the computational simplicity and efficiency of finite differences. It is globally second-order accurate and especially developed for the resolution of steep fronts arising when advective fluxes are dominating the process.

The paper is organized as follows. First, the finite volume scheme is developed with reference to triangular control volumes, and the convective and dispersive fluxes are derived. A short review is proposed on the one-dimensional Godunov's scheme and its higher-order extensions, upon which the high-resolution upwind scheme is based. The high-resolution upwind scheme, defined in terms of Godunov's method, is applied to triangular control volumes. The discretization of the dispersive fluxes, together with the forcing function, is then reported. Finally the description of the time stepping technique, and the operational definition of the Courant number, the Peclet number and the stability criteria close the analytical developments.

The second part of the paper discusses some numerical results obtained with the proposed approach. To demonstrate the robustness of the scheme, examples regarding the solution of the one- and two-dimensional transport equations are discussed. Purely dispersive cases are treated as well as purely hyperbolic problems, and linear and nonlinear forcing functions are considered.

THE FINITE VOLUME APPROACH

The contaminant transport equation in groundwater can be generally written as [*Bear*, 1979]:

$$\theta \frac{\partial c}{\partial t} + \nabla \cdot (\theta \mathbf{v} c) = \nabla \cdot (\theta \mathbf{D} \nabla c) + G \tag{1}$$

where

- c concentration of the contaminant;
- θ porosity of the porous medium;
- $\mathbf{v}$ velocity field;
- ∇ gradient operator;
- $\mathbf{D}$ dispersion tensor.

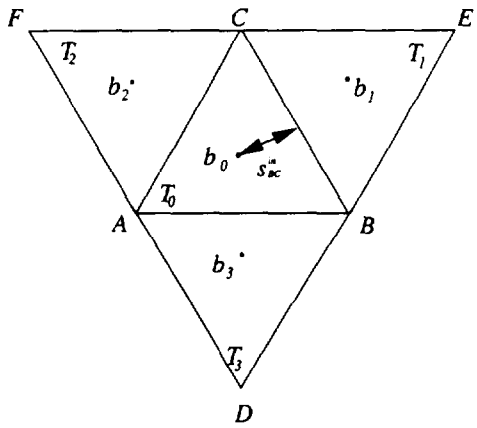

Fig. 1. Triangular control volumes used in the derivation of the convective and dispersive numerical fluxes.

The term G represents all the sources or sinks and all the transformations that the contaminant may undergo. A simplified, two-dimensional model problem is used for the derivation of the finite volume scheme:

$$\frac{\partial c}{\partial t} + \nabla \cdot \mathbf{F} = \nabla \cdot \mathbf{D} \nabla c + G \tag{2}$$

where $\mathbf{F} = \mathbf{v}c$ is the advective flux vector.

The scheme is defined over triangular control volumes (Figure 1) over which the dependent variable c is averaged. For the space discretization, (2) is integrated over triangle T_0 with area A_{T_0}:

$$\int_{T_0} \frac{\partial c}{\partial t} d\mathbf{x} + \int_{T_0} \nabla \cdot \mathbf{F} d\mathbf{x} = \int_{T_0} \nabla \cdot \mathbf{D} \nabla c d\mathbf{x} + \int_{T_0} G d\mathbf{x} \tag{3}$$

Interchanging the time differentiation and the space integration operators, the equation can be written as

$$\frac{\partial}{\partial t} c_{ABC} = \frac{1}{A_{T_0}} \left[- \int_{T_0} \nabla \cdot \mathbf{F} d\mathbf{x} + \int_{T_0} \nabla \cdot \mathbf{D} \nabla c \, d\mathbf{x} + \int_{T_0} G d\mathbf{x} \right] \tag{4}$$

$$c_{ABC} = \frac{1}{A_{T_0}} \int_{T_0} c d\mathbf{x}$$

The variable c_{ABC} becomes the new dependent variable and its value is assigned to the centroid of T_0.

Application of the divergence theorem to (4) gives

$$\begin{aligned} \frac{\partial}{\partial t} c_{ABC} = -\frac{1}{A_{T_0}} \Bigg\{ \Bigg[& \int_{AB} \mathbf{F} \cdot \hat{\mathbf{n}}_{AB} \, ds + \int_{BC} \mathbf{F} \cdot \hat{\mathbf{n}}_{BC} \, ds \\ & + \int_{CA} \mathbf{F} \cdot \hat{\mathbf{n}}_{CA} \, ds \Bigg] - \Bigg[\int_{AB} \mathbf{D} \nabla c|_{AB} \cdot \hat{\mathbf{n}}_{AB} \, ds \\ & + \int_{BC} \mathbf{D} \nabla c|_{BC} \cdot \hat{\mathbf{n}}_{BC} \, ds + \int_{CA} \mathbf{D} \nabla c|_{CA} \cdot \hat{\mathbf{n}}_{CA} \, ds \\ & + \int_{T_0} G dx \Bigg] \Bigg\} \end{aligned} \tag{5}$$

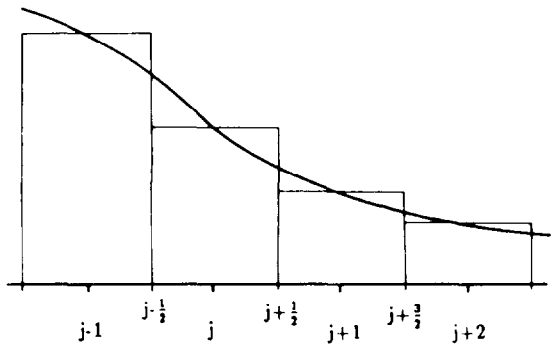

Fig. 2. Piecewise constant interpolation of the dependent variable c.

where F_{AB}, F_{BC}, and F_{CA} are the convective fluxes and $\mathbf{D}\nabla c|_{AB}$, $\mathbf{D}\nabla c|_{BC}$, and $\mathbf{D}\nabla c|_{CA}$ are the dispersive fluxes across the sides of triangle T_0, and $\hat{\mathbf{n}}_{AB}$, $\hat{\mathbf{n}}_{BC}$, and $\hat{\mathbf{n}}_{CA}$ are the unit outward normal vectors for each side of T_0. The semidiscrete version of the previous equation can be written

$$\frac{\partial}{\partial t} c_{ABC} = -\frac{1}{A_{T_0}} \{-[\hat{f}_{AB} + \hat{f}_{BC} + \hat{f}_{CA}] + [\hat{D}_{AB} + \hat{D}_{BC} + \hat{D}_{CA}] + \hat{G}\} \quad (6)$$

where $\hat{f}$ and $\hat{D}$ represent the space discretization operators for, respectively, the convective fluxes and the dispersive fluxes, and $\hat{G}$ represents the forcing functions.

Convective Fluxes

The calculation of the numerical convective flux is based on an extension of Godunov-type schemes to triangular control volumes. Godunov's scheme, and its higher-order extensions can be exemplified by simple applications to one-dimensional scalar hyperbolic equations. For the following discussion, the reader is referred to the reviews by *Sweby* [1985] and *Goodman and LeVeque* [1988]; the approach used is taken from *van Leer* [1977*a*, *b*].

Godunov's scheme. Consider the one-dimensional scalar hyperbolic equation in conservation form:

$$\frac{\partial c}{\partial t} + \frac{\partial f(c)}{\partial x} = 0 \quad (7)$$

subject to appropriate initial and boundary conditions. Define the computational grid by means of cell centers $x_j = (j = \frac{1}{2})\Delta x$, $(j = 1, \cdots, J)$, and cell interfaces $x_{j+1} = j\Delta x$, $(j = 0, 1, \cdots, J)$, in space, and $t_n = n\Delta t$, $n = 1, 2, \cdots, N$ in time. Let $\bar{c}_j^n$ be the interpolation of the dependent variable c over each interval $(x_{j-(1/2)}, x_{j+(1/2)})$ by a piecewise constant function at time t_n (Figure 2):

$$\bar{c}_j^n = \frac{1}{\Delta x} \int_{x_{j-(1/2)}}^{x_{j+(1/2)}} c(x, t_n)\, dx \quad (8)$$

Godunov's scheme proceeds as follows. First at each cell interface the analytical solution $c^e(x_{j+(1/2)}, t)$ to the local so-called Riemann problem is calculated for $t_n < t < t_{n+1}$. This local problem is constituted by (7) defined over a domain which extends indefinitely on both parts of the cell interface. The initial conditions are given by the constant states (8) calculated in the two neighboring control volumes and extended over the infinite domain. The solution of the local Riemann problem at the interface $x_{j+(1/2)}$ between cells j and $j + 1$ yields a state $c^e(c_{j+(1/2)}, t)$ which is used to evaluate the numerical flux:

$$\hat{f}_{j+(1/2)}^n = \frac{1}{\Delta t} \int_{t_n}^{t_{n+1}} f(c^e(x_{j+(1/2)}, \tau))\, d\tau \quad (9a)$$

The new state at t_{n+1} becomes

$$\bar{c}_j^{n+1} = \bar{c}_j^n - \frac{\Delta t}{\Delta x} (\hat{f}_{j+(1/2)}^n - \hat{f}_{j-(1/2)}^n) \quad (9b)$$

A forward Euler time stepping scheme approximates (9) by

$$\hat{f}_{j+(1/2)}^n = f(c^e(x_{j+(1/2)}, t_n)) \quad (10)$$

and leads to first-order accuracy in time. For a linear flux, $f = vc$, as usually encountered in groundwater transport of monophasic contaminants, (9) simplifies to:

$$\hat{f}_{j+(1/2)}^n = v_j \bar{c}_j^n \qquad v_j > 0$$
$$\hat{f}_{j+(1/2)}^n = v_{j+1} \bar{c}_{j+1}^n \qquad \text{otherwise} \quad (11)$$

It is easy to show that Godunov's scheme is only first-order accurate in space, and that the stability condition for this method requires that the Courant-Friedrichs-Lewy (CFL) number be less than unity. The CFL number can be defined for (7) as $CFL = (\Delta t/\Delta x)|\max f'(c)|$, or $CFL = (\Delta t/\Delta x)|v|$ for a linear flux. The advantage of this scheme in solving hyperbolic equations stems from the fact that, whenever stability is ensured, it is free of numerical oscillations. In fact the total variation (TV) of the discrete solution, defined as:

$$TV(\bar{c}_j^n) = \sum_{j=0}^{J} |\bar{c}_{j+1}^n - \bar{c}_j^n| \quad (12)$$

is a nonincreasing function of time:

$$TV(\bar{c}_j^{n+1}) \le TV(\bar{c}_j^n) \quad (13)$$

This statement implies that no oscillations are artificially created by the scheme when starting from nonoscillatory initial data. This property is generally indicated as TVNI (total variation nonincreasing) or, less appropriately, as TVD (total variation diminishing).

Second-order spatial accuracy. Second-order extensions are obtained by employing piecewise linear interpolation, as opposed to piecewise constant, for the calculation of the numerical fluxes at each cell interface. However, care must be exercised: in order to avoid oscillations the interpolation must be performed in a monotonic way. This is accomplished by imposing the interpolated variable in each cell to be bounded by the value of the same variable in neighboring cells. The slope of the linear distribution inside the control volume must therefore be changed according to neighboring values. In the presence of a local or global maximum the slope is set to zero. This procedure is called "limiting" and is automatically carried out only where the

solution displays large gradients; i.e., where the data at the last time level are not smooth.

The discrete operator of this second order Godunov-type scheme can be summarized in three distinct phases: (1) reconstruction using linear interpolation (R) plus limiting (L); (2) evolution (solution to the local Riemann problem) (E); and (3) average (projection on the original grid by cell averaging the result of evolution) (A). These three steps can be visualized graphically as in Figure 3 in the case of linear advection.

The definition of the evolution and averaging operators is immediate once the reconstruction operator, and hence the numerical fluxes across cell interfaces, are known. Let us look then first at the reconstruction operator.

Let $\Delta c_{j+(1/2)} = c_{j+1} - c_j$ and denote by $\Delta c_j = \frac{1}{2}(\Delta c_{j+(1/2)} + \Delta c_{j-(1/2)})$ the average gradient in cell j (e.g., $\Delta c_j = \frac{1}{2}(c_{j+1} - c_{j-1})$). Then the linear reconstruction operator may be expressed as

$$R_j^n(x) = \bar{c}_j^n + \left(\frac{x - x_j}{\Delta x}\right)\overline{\Delta c}_j^n \qquad \left|\frac{x - x_j}{\Delta x}\right| < \frac{1}{2}$$
$$R_j^n(x) = 0 \qquad \text{otherwise} \tag{14}$$

Here Δc_j^n is the average gradient in cell j, changed by the limiting procedure. Limiting is required to obtain a monotone reconstruction. It should be noted that the reconstruction $R^n(x) = V_j R_j^n(x)$ itself does not have to be monotone, but the result after evolution and averaging must be. This can be clarified by an example using linear advection. We now apply the evolution operator to the reconstruction data result in $R^n(x - v(t^{n+1} - t^n))$, where v is the constant velocity field. The new solution becomes:

$$\bar{c}_j^{n+1} = \frac{1}{\Delta x}\int_{x_{j-(1/2)}}^{x_{j+(1/2)}} R^n(x - v(t^{n+1} - t^n))\, dx \tag{15}$$

Define $\xi = x_j - v(t^{n+1} - t^n)$ and find i such that $\xi \in [x_i, x_{i+1}]$. Then (15) results in

$$\bar{c}_j^{n+1} = \bar{c}_i^n + \frac{(\xi - x_i)}{\Delta x}\Delta c_{i+(1/2)}^n + \frac{1}{2}\frac{(\xi - x_i)(\xi - x_{i+(1/2)})}{(\Delta x)^2}(\overline{\Delta c}_{i+1}^n - \overline{\Delta c}_i^n) \tag{16}$$

This expression will be monotone in ξ only if

$$|\Delta c_{i+1}^n - \Delta c_i^n| \le 2|\Delta c_{j+(1/2)}^n| \tag{17}$$

In general this condition is not satisfied if the interpolated data are not smooth, and the average gradients in the third term of the right-hand side of (16) must be changed. This is obtained by the limiting procedure is such a way that the limited gradient $\overline{\Delta c}^n$ satisfies condition (17). The resulting slope is changed until the dependent variable agrees with the average values found at each cell interface as shown in Figure 3*b*. This variation in the slope of the linear distribution of the dependent variable introduces some numerical diffusion. The goal is then to provide a limiting rule that will act only on nonsmooth parts of the solution and will add the least amount of artificial diffusion when sharp fronts are detected.

For this purpose, define the smoothness parameter:

$$r_j = \frac{\Delta c_{j-(1/2)}}{\Delta c_{j+(1/2)}} \tag{18}$$

as the ratio between two consecutive gradients, and let the limited flux $\overline{\Delta c}$ be:

$$\overline{\Delta c}_j^n = \phi(r_j)\Delta c_{j+(1/2)}^n = \phi\left(\frac{1}{r_j}\right)\Delta c_{j+(1/2)}^n \tag{19}$$

where $\phi(r_j)$ is the "limiting function" or simply "limiter." When $r_j \to 1$, which means that the numerical solution is smooth, the limiting function must evidently approach unity. In any case the limiter must conserve second-order accuracy and the TVNI property of the scheme. It can be shown [*Sweby*, 1984] that, in the linear case, and with the appropriate time stepping, we recover the well-known second-order accurate Lax-Wendroff method if $\phi(r) = 1$. A second-order TVNI scheme may be in fact viewed as obtained through a redefinition of the Lax-Wendroff numerical flux using the limiting procedure.

Many different choices of ϕ allow second-order accuracy together with TVNI. One simple formula is given by *Roe*'s [1986] "minmod" function, defined as:

$$\phi(r) = \max[0, \min(r, 1)] \tag{20}$$

Using $r = x/y$ with $x = \Delta c_{j+(1/2)}^n$ and $y = \Delta c_{j-(1/2)}^n$ we obtain

$$\phi\left(\frac{y}{x}\right) = \text{minmod}(x, y) = \text{sign}(x)\max\{0, \min[|x|, y\,\text{sign}(x)]\} \tag{21}$$

which may be rewritten as:

$$\text{minmod}(x, y) = x \text{ if } |x| \le |y|$$
$$\text{minmod}(x, y) = y \text{ if } |x| > |y| \tag{22}$$
$$\text{minmod}(x, y) = 0 \text{ if } xy \le 0$$

For a more exhaustive discussion on limiters the reader is referred to the paper by *Sweby* [1984].

For nonlinear problems, the evolution operator in (15) does not have a simple form. Therefore, we use (9) based on fluxes. The time integration will be approximated by a second-order accurate two-step scheme to be described later. The scheme requires fluxes computed from the solution of the local Riemann problem. With the piecewise linear reconstruction, the numerical flux takes the form [*Chakravarthy and Osher*, 1985]:

$$\hat{f}_{j+(1/2)} = \frac{1}{2}[f(\tilde{c}_{j+(1/2)}^+) + f(\tilde{c}_{j+(1/2)}^-)] - \frac{1}{2}[df_{j+(1/2)}^+ - df_{j+(1/2)}^-] \tag{23}$$

where $f(\tilde{c})$ is the general convective flux,

$$df_{j+(1/2)}^+ = \max[\text{sign}(v_j), 0][f(\tilde{c}_{j+(1/2)}^+) - f(\tilde{c}_{j+(1/2)}^-)] \tag{24a}$$

$$df_{j+(1/2)}^- = -\min[\text{sign}(v_j), 0][f(\tilde{c}_{j+(1/2)}^+) - f(\tilde{c}_{j+(1/2)}^-)] \tag{24b}$$

$$\tilde{c}_{j+(1/2)}^- = c_j + \frac{1}{2}\overline{\Delta c}_j \tag{24c}$$

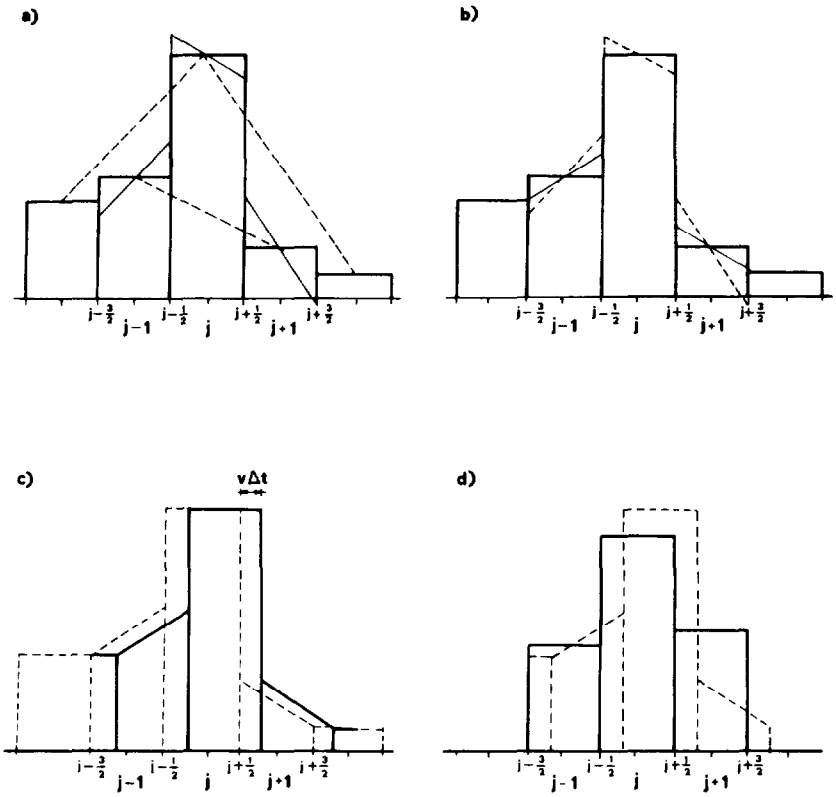

Fig. 3. Graphical visualization of one step of a second order Godunov-type scheme for linear advective flux: (*a*) reconstruction; (*b*) limiting; (*c*) evolution (solution to local Riemann problem); (*d*) average.

$$\bar{c}^{+}_{j+(1/2)} = c_{j+1} - \frac{1}{2}\overline{\Delta c}_{j+1} \tag{24d}$$

and $\overline{\Delta c}_j$ is given by (19). Here $\bar{c}^{-}_{j+(1/2)}$ is the limited value of the linear interpolation of $\bar{c}_j$ in $x_{1+(1/2)}$, while $\bar{c}^{+}_{j+(1/2)}$ is the limited value of the linear interpolation of $\bar{c}_{j+1}$ in $x_{j+(1/2)}$. In case of a linear flux, (23) takes a simpler form:

$$\hat{f}_{j+(1/2)} = \frac{1}{2}\left[f(\bar{c}^{+}_{j+(1/2)}) + f(\bar{c}^{-}_{j+(1/2)})\right] - \frac{1}{2}\,\text{sign}\,(v_j)\left[f(\bar{c}^{+}_{j+(1/2)}) - f(\bar{c}^{-}_{j+(1/2)})\right] \tag{25}$$

Hence for $f(c) = vc$,

$$\hat{f}_{j+(1/2)} = \frac{1}{2}\left\{v_{j+1}\bar{c}^{+}_{j+(1/2)} + v_j\bar{c}^{-}_{j+(1/2)} - \text{sign}\,(v_j)\left[v_j\bar{c}^{-}_{j+(1/2)} - v_{j+1}\bar{c}^{+}_{j+(1/2)}\right]\right\} \tag{26}$$

or in equivalent form,

$$\begin{aligned} \hat{f}_{j+(1/2)} &= v_j\bar{c}^{-}_{j+(1/2)} \qquad v_j < 0 \\ \hat{f}_{j+(1/2)} &= v_{j+1}\bar{c}^{+}_{j+(1/2)} \qquad \text{otherwise} \end{aligned} \tag{27}$$

This expression represents the exact solution to the local Riemann problem,

$$\frac{\partial c}{\partial t} + v\frac{\partial c}{\partial x} = 0 \tag{28}$$

across the cell interface $j + 1$ with initial conditions given by

$$\begin{aligned} c &= \bar{c}^{-}_{j+(1/2)} \qquad x < x_{j+(1/2)} \\ c &= \bar{c}^{+}_{j+(1/2)} \qquad x > x_{j+(1/2)} \end{aligned} \tag{29}$$

and velocity field

$$\begin{aligned} v &= \bar{v}^{-}_{j} \qquad x < x_{j+(1/2)} \\ v &= \bar{v}^{+}_{j+1} \qquad x > x_{j+(1/2)} \end{aligned} \tag{30}$$

Note that the original first-order scheme is obtained by setting $\overline{\Delta c}_j$ in (24) to zero for cell j. If Δc_j is computed through a limiter, the scheme is globally second-order accurate and TVNI. Second-order accuracy is obtained almost everywhere except at sharp fronts, where the limiter forces first-order ($O(\Delta x)$) errors. However, this behavior does not destroy the global accuracy of the solution which remains of second order. The particular monotone interpolation used in the reconstruction phase guarantees the solution to be TVNI by adding first-order numerical diffusion at discontinuities only.

Many different limiters have been proposed in the literature, each of them having different properties. However, this

point is not essential for the present discussion as long as the limiter employed in the calculations lies in the second-order accuracy region.

Higher-order schemes can be obtained employing more accurate interpolation of the dependent variable. However, the definition of the appropriate limiters becomes more complex.

Extension to triangular control volumes. The application of the second-order upwind scheme to two spatial dimensions is immediate for rectangular control volumes. In this case, one can split the fluxes along the directions orthogonal to each cell boundary. Then the reconstruction and flux computation for the one-dimensional problem can be applied to each direction and combined together in a finite volume fashion similar to (6). The numerical flux at each cell interface is then given by (23) and (24).

The use of triangular control volumes requires a more complex formulation. In particular the interpolation of the dependent variable from the centroid to the sides of the triangle is now a two-dimensional process. Once the interpolated values at each side are obtained, limiting and evolution can again be performed as in the one-dimensional case.

Consider the equilateral triangle T_0 of Figure 1, formed by the vertices A, B, and C. Let B_0 be the centroid of T_0 and let T_1, T_2, and T_3 be the neighboring triangles with b_1, b_2, and b_3 their respective centroids. Let us focus on the derivation of the numerical flux $\hat{f}_{BC}$ across side BC; the fluxes across the other sides of T_0 are derived analogously.

Let c_{ABC} be the value of the dependent variable in b_0, and let $\bar{c}^{\text{in}}_{BC}$ be the interpolation of c_{ABC} to the side BC. The superscript "in" indicates that the interpolation is performed from the "inside" of T_0 with respect to BC. Analogously the superscript "out" indicates that the interpolation is performed from the "outside" of T_0. Note that the "inside" for T_0 corresponds to the "outside" for T_1, and vice versa.

The value of $\bar{c}^{\text{in}}_{BC}$ can be calculated as

$$\bar{c}^{\text{in}}_{BC} = c_{ABC} + s^{\text{in}}_{BC}\left(\frac{\overline{\partial c}}{\partial n}\right)^{\text{in}}_{BC} \tag{31}$$

where s^{in}_{BC} is the distance of b_0 from side BC and n is the direction normal to BC. To evaluate the normal derivative at side BC the divergence theorem is used: the derivative c can be calculated as

$$A_{T_0}\frac{\overline{\partial c}}{\partial n} = \int_{T_0}\frac{\partial c}{\partial n}\,dx\,dy = \oint_{T_0} c\mathbf{n}\,ds \tag{32}$$

where s is the linear coordinate along the perimeter of T_0. Note that $c^{\text{in}}_{AB} = c^{\text{in}}_{BC} = c^{\text{in}}_{CA}$ and

$$\overline{BC} + \overline{AB}\hat{\mathbf{n}}_{AB}\cdot\hat{\mathbf{n}}_{BC} + \overline{CA}\hat{\mathbf{n}}_{CA}\cdot\mathbf{n}_{BC} = 0 \tag{33}$$

where $\hat{\mathbf{n}}$ is the unit outward normal to the corresponding side. Given the differences

$$\alpha_{AB} = c^{\text{out}}_{AB} - c^{\text{in}}_{AB}$$

$$\alpha_{BC} = c^{\text{out}}_{BC} - c^{\text{in}}_{BC}$$

$$\alpha_{CA} = c^{\text{out}}_{CA} - c^{\text{in}}_{CA}$$

and (33), the integral (32) can be calculated numerically in two ways: (1) by slightly shifting T_0 to one side of BC:

$$A_{T_0}\left(\frac{\overline{\partial c}}{\partial n}\right)^{(1)}_{BC} = \overline{BC}c^{\text{out}}_{BC} + \overline{AB}c^{\text{in}}_{AB}\hat{\mathbf{n}}_{AB}\cdot\hat{\mathbf{n}}_{BC} + \overline{CA}c^{\text{in}}_{CA}\hat{\mathbf{n}}_{CA}\cdot\hat{\mathbf{n}}_{BC}$$

$$= \overline{BC}\alpha_{BC} \tag{34}$$

and (2) by slightly shifting T_0 to the other side of BC:

$$A_{T_0}\left(\frac{\overline{\partial c}}{\partial n}\right)^{(2)}_{BC} = \overline{BC}c^{\text{in}}_{BC} + \overline{AB}c^{\text{in}}_{AB}\hat{\mathbf{n}}_{AB}\cdot\hat{\mathbf{n}}_{BC} + \overline{CA}c^{\text{out}}_{CA}\hat{\mathbf{n}}_{CA}\cdot\hat{\mathbf{n}}_{BC}$$

$$= \overline{AB}\alpha_{AB}\hat{\mathbf{n}}_{AB}\cdot\hat{\mathbf{n}}_{BC} + CA\alpha_{CA}\hat{\mathbf{n}}_{CA}\cdot\hat{\mathbf{n}}_{BC} \tag{35}$$

The average of $(\overline{\partial c}/\partial n)^{(1)}_{BC}$ and $(\overline{\partial c}/\partial n)^{(2)}_{BC}$ gives a first-order approximation to $(\overline{\partial c}/\partial n)^{\text{in}}_{BC}$, that may be interpreted as the average gradient of the dependent variable across side BC. Hence (34) and (35) can be used as arguments of the limiting process to get the following second-order flux-limited approximation:

$$\left(\frac{\overline{\partial c}}{\partial n}\right)^{in}_{BC} = \{\text{minmod}\,[\overline{BC}\alpha_{BC}, \overline{AB}\alpha_{AB}\hat{\mathbf{n}}_{AB}\cdot\hat{\mathbf{n}}_{BC}$$

$$+ \overline{CA}\alpha_{CA}\hat{\mathbf{n}}_{CA}\cdot\hat{\mathbf{n}}_{BC}]\}A^{-1}_{T_0} \tag{36}$$

The general numerical convective flux can now be written in full as

$$\hat{f}_{BC} = \frac{1}{2}\left[\mathbf{F}(\bar{c}^{\text{in}}_{BC})\cdot\mathbf{n}_{BC} + \mathbf{F}(\bar{c}^{\text{out}}_{BC})\cdot\mathbf{n}_{BC} - (df^{+}_{BC} - df^{-}_{BC})\right] \tag{37a}$$

where $\mathbf{n}_{BC} = \overline{BC}\hat{\mathbf{n}}_{BC}$, $\hat{\mathbf{n}}_{BC}$ is the unit outward normal to side BC,

$$df^{+}_{BC} = \max\,[\text{sign}\,(\mathbf{v}^{\text{in}}_{ABC}\cdot\hat{\mathbf{n}}_{BC}), 0][f(\bar{c}^{\text{out}}_{BC}) - f(\bar{c}^{\text{in}}_{BC})] \tag{37b}$$

$$df^{-}_{BC} = -\min\,[\text{sign}\,(\mathbf{v}^{\text{in}}_{ABC}\cdot\hat{\mathbf{n}}_{BC}), 0][f(\bar{c}^{\text{out}}_{BC}) - f(\bar{c}^{\text{in}}_{BC})] \tag{37c}$$

and $f_{BC}(\ ) = \mathbf{F}_{BC}(\ )\cdot\mathbf{n}_{BC}$. Note how the expressions in (37b) and (37c) are immediate extensions of equations (24a) and (24b) in the one-dimensional case.

In the case of linear flux, since $\mathbf{F} = \mathbf{v}c$, and $f = \mathbf{v}c\cdot\mathbf{n}$, we obtain an expression similar to (27) which represents the solution to the local Riemann problem:

$$\hat{f}_{BC} = \bar{c}^{\text{in}}_{BC}\mathbf{v}^{\text{in}}_{ABC}\cdot\hat{\mathbf{n}}_{BC} \qquad \mathbf{v}^{\text{in}}_{BC} > 0$$

$$\hat{f}_{BC} = \bar{c}^{\text{out}}_{BC}\mathbf{v}^{\text{out}}_{ABC}\cdot\hat{\mathbf{n}}_{BC} \qquad \text{otherwise} \tag{38}$$

The proposed scheme introduces first-order numerical viscosity only where sharp concentration fronts are encountered. In smooth regions of the solution, only second-order numerical diffusion is added. Because the TVNI property is insured, the technique is free of spurious oscillations even in the presence of discontinuities. The formulation is globally second-order accurate when applied to equilateral triangular grids. It will remain certainly second order as long as (31) holds, that is, as long as the distance of the centroids from the sides of each cell varies within the order of the spatial truncation error, $O(\Delta x^2)$. Therefore nonuniform grids may be used, but the transition from the equilateral shape and from element to element must be smooth. Schemes that are of global second-order accuracy in any situation can be

obtained, but seem to lose the appealing simplicity of the present formulation.

Any other second-order accurate limiting technique besides "minmod" can be employed, but it must account for the triangular form of the control volume. Among the many limiters presented in the literature, minmod is the one that introduces the largest amount of numerical viscosity, but it is the most robust, and does not require particular attention for its use in two-dimensional triangular cells. Sharper concentration fronts could probably be obtained employing different limiters, but their definition on triangular cells is not immediate. The study and use of different limiters is one of the issues that will be pursued in future research.

Dispersive Fluxes

The dispersive fluxes and the forcing functions are represented by the second part of (5). For triangle T_0 they can be written as:

$$D_{ABC} = \frac{1}{A_{T_0}}\left[\int_{AB} \mathbf{D}\nabla c|_{AB}\cdot\hat{\mathbf{n}}_{AB}\,ds + \int_{BC} \mathbf{D}\nabla c|_{BC}\cdot\hat{\mathbf{n}}_{BC}\,ds + \int_{CA} \mathbf{D}\nabla c|_{CA}\cdot\hat{\mathbf{n}}_{CA}\,ds + \int T_0 G dx\right]$$

$$= \frac{1}{A_{T_0}}[\hat{D}_{AB} + \hat{D}_{BC} + \hat{D}_{CA} + \hat{G}] \tag{39}$$

For each side of the control volume, approximations to the normal derivative and the tangential derivative can be defined. These are then projected along the coordinate axis, multiplied by the dispersion tensor, and then projected along the direction normal to the side. For example, for side BC, the normal derivative can be approximated by

$$\left(\frac{\partial c}{\partial n}\right)_{BC} = \frac{c_1 - c_0}{\overline{b_1 b_0}} \tag{40}$$

where $\overline{b_1 b_0}$ is the distance between the centroids of triangles T_1 and T_0. The tangential derivative can be written as

$$\left(\frac{\partial c}{\partial s}\right)_{BC} = \frac{\bar{c}_B - \bar{c}_C}{\overline{BC}} \tag{41}$$

in which $\bar{c}_B$ and $\bar{c}_C$ are defined as

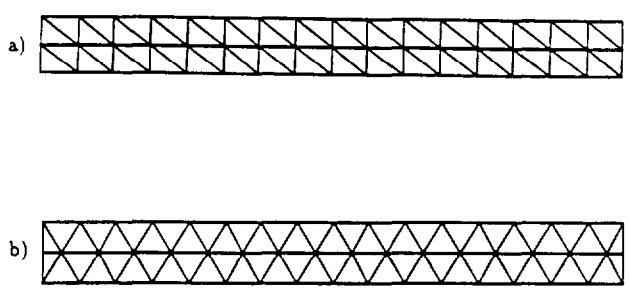

Fig. 4. Computational grids used in the one-dimensional simulations.

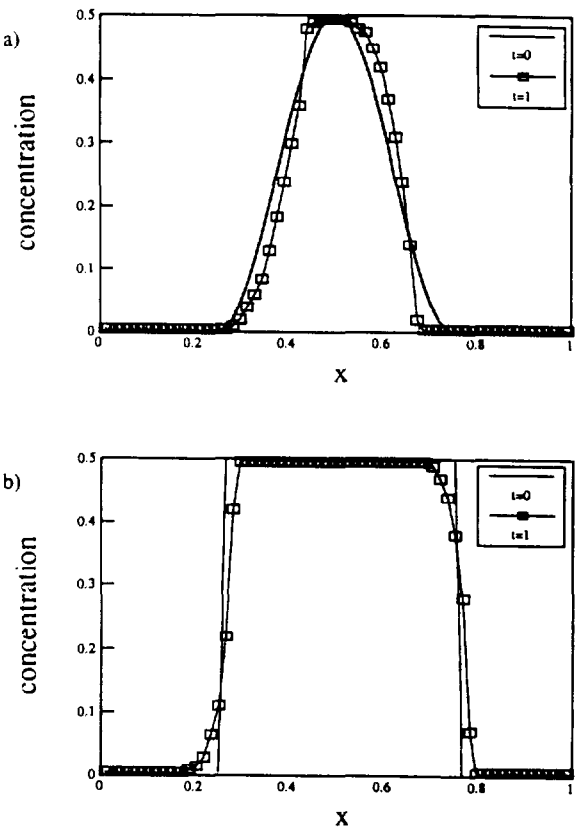

Fig. 5. Purely advective example. Initial conditions and concentration profiles obtained after one period with the second order accurate in time and space for $CFL = 0.5$: (*a*) $\sin^2$ wave; (*b*) square wave for $\Delta x = 1/64$.

$$\bar{c}_B = \sum_{j=1}^{N_B} A_{T_j} c_j \Big/ \sum_{j=1}^{N_B} A_{T_j} \qquad \bar{c}_C = \sum_{j=1}^{N_C} A_{T_j} c_j \Big/ \sum_{j=1}^{N_C} A_{T_j} \tag{42}$$

where N_B and N_C are the number of triangles T_j that have respectively nodes B and C in common, and c_j is the value of the concentration in triangle T_j. The dispersive fluxes can then be evaluated by

$$\hat{D}_{BC} = (\mathbf{D}\hat{\nabla} c|_{BC})\cdot\hat{n}_{BC}\overline{BC} \tag{43}$$

where $\hat{\nabla} c|_{BC}$ is evaluated from equations (40) and (41) by projection along the coordinate axis:

$$\hat{\nabla} c|_{BC} = \left[\left(\frac{\partial c}{\partial x}\right)_{BC}, \left(\frac{\partial c}{\partial y}\right)_{BC}\right]^T \tag{44}$$

Equation (43) is a consistent approximation to the dispersive fluxes. It is locally first-order accurate but achieves global second-order accuracy on the whole domain as long as the triangulation does not become too irregular.

Time Discretization and Stability

A peculiar characteristic of the high-order upwind scheme adopted for the discretization of the convective fluxes is that it is intrinsically nonlinear even when applied to a linear equation, as in the present case. Also, it can be shown that the scheme is unconditionally unstable when a first-order approximation to the time derivative is used. For this

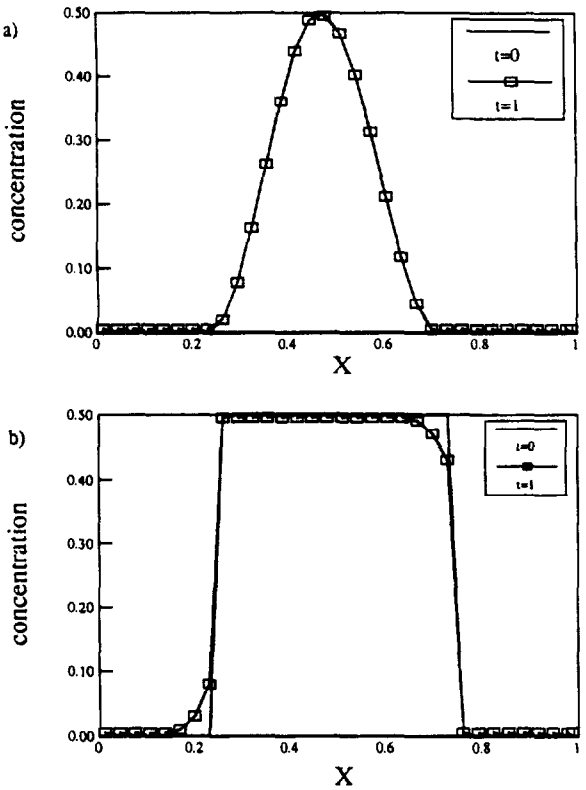

Fig. 6. Purely advective example. Initial conditions and concentration profiles obtained after one period with the second order accurate in time and space for $CFL = 0.9$: (*a*) $\sin^2$ wave; (*b*) square wave for $\Delta x = 1/32$.

reason, Hancock's scheme [*van Albada et al.*, 1982] is employed. It is a two-step second-order accurate explicit scheme.

Denoting by $\hat{\mathbf{R}}$, the right-hand side of (6), the technique can be written as

$$c^{n+(1/2)} = c^n - \frac{1}{2}\Delta t \hat{\mathbf{R}}^*(c^n)$$
$$c^n = c^n - \Delta t \hat{\mathbf{R}}(c^{n+(1/2)}) \tag{45}$$

The superscript n denotes the time stage ($0 \le n \le N$) and Δt is the time spacing. In the first half step, the asterisk denotes that the convective flux is evaluated using values inside the control volume, interpolated from the centroid to the boundary of the cell but evolution is not performed. While for the dispersive fluxes the scheme is a normal second-order Runge-Kutta technique, for the convective fluxes the Riemann problem is not solved on the first half step, thereby achieving better efficiency.

Limitations on the size of the time step must be satisfied to ensure stable solutions. For the proposed triangular control volumes, it is necessary to redefine the Courant-Friedrichs-Lewy number (CFL) and the diffusion number (γ).

For the linear convective flux the CFL number can be defined as

$$CFL = \frac{1}{2}\frac{\oint_{T_0} |\mathbf{v}\cdot\mathbf{n}|\, ds}{A_{T_0}}\Delta t \tag{46}$$

and the diffusion number γ as

$$\gamma = \frac{|\mathbf{D}|\Delta t}{A_{T_0}} \tag{47}$$

where $|\mathbf{D}|$ represents a vector or matrix norm of $\mathbf{D}$. Numerical experiments suggest that the following standard criterion is sufficient for stability:

$$\max[\mathbf{CFL}, 2\gamma] < 1 \tag{48}$$

In the same fashion, we can define the cell-Peclet number to be

$$Pe = \frac{CFL}{\gamma} = \frac{\oint_{T_0} |\mathbf{v}\cdot\mathbf{n}|\, ds}{2|\mathbf{D}|} \tag{49}$$

As in the standard case, when Pe is small the equation is dominated by dispersion phenomena; when large, advective terms prevail.

The size of the allowable time step can be severely limited by stability condition (48) when γ is large. The computational efficiency of the scheme may become very low in this case. The use of second-order accurate implicit schemes

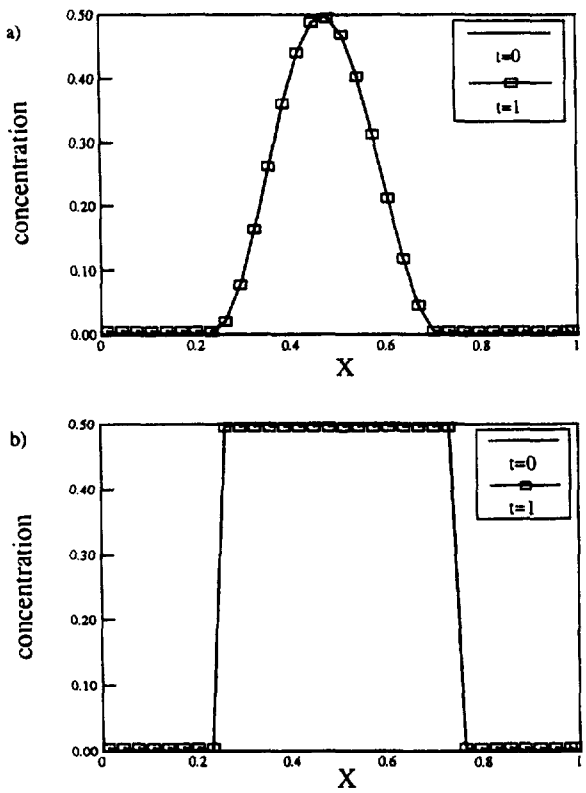

Fig. 7. Purely advective example. Initial conditions and concentration profiles obtained after one period with the second order accurate in time and space for $CFL = 1.0$: (*a*) $\sin^2$ wave; (*b*) square wave for $\Delta x = 1/32$.

increases the maximum Δt, which is now limited only by accuracy requirements, although a set of nonlinear equations must be solved even for linear convective fluxes. However, it can be shown that the proposed scheme produces diagonally dominant matrices, and hence efficient relaxation schemes can be derived. The solution of the nonlinear system can be obtained by means of Picard iterations.

NUMERICAL EXAMPLES

One-Dimensional Simulation

To test the accuracy and the general behavior of the scheme, the following one-dimensional constant coefficient advection-diffusion problem is solved in a two-dimensional grid system using different dimensionless parameters:

$$\frac{\partial c}{\partial t} + \nabla \cdot \mathbf{F} = \nabla \cdot \mathbf{D}\nabla c$$
$$\mathbf{F} = \mathbf{v}c \tag{50}$$

A rectangular domain with unitary length is discretized using rectangular and equilateral triangles (Figure 4) so that the effects of the shape of the control volume on the numerical solution can be evaluated. Two different grid spacings are used for the calculations: $\Delta x_1 = 1/32$ and $\Delta x_2 = 1/64$ corresponding, respectively, to discretizations formed by 33 and 65 elements. The size of the time step is calculated according to (48). In the experiments conducted, only very small differences

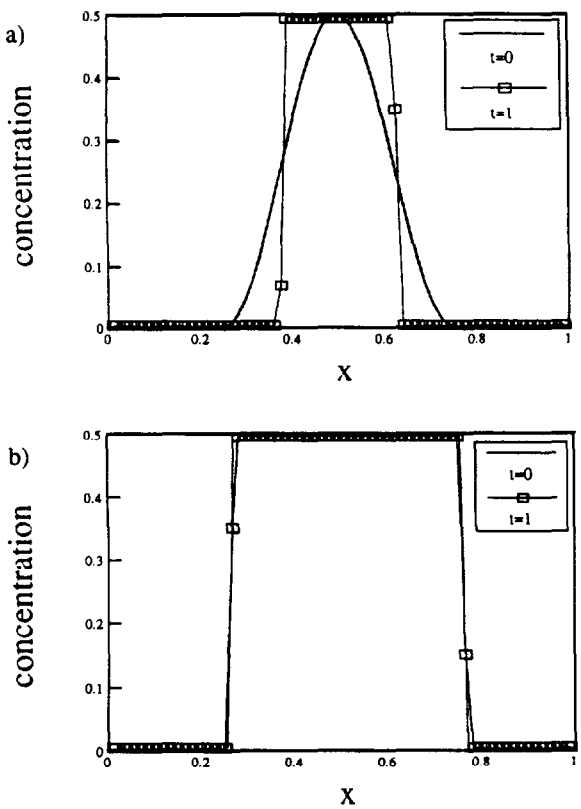

Fig. 8. Purely advective example. Initial conditions and concentration profiles obtained after one period with the second order accurate in time and space: (*a*) $\sin^2$ wave; (*b*) square wave for $\Delta x = 1/64$.

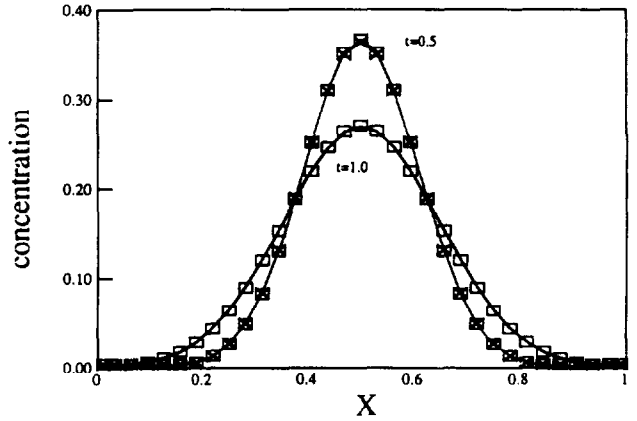

Fig. 9. Purely diffusive example. Concentration profiles and analytical solutions at $t = 0.5$ and $t = 1.0$ for $\Delta x = 1/32$.

can be noted in the numerical solutions obtained from the two grid systems. This fact suggests that the scheme will remain second-order accurate as long as the shape of the elements is not much different from the equilateral.

The first example problem is an application to a purely hyperbolic equation with constant coefficients and linear flux:

$$\frac{\partial c}{\partial t} + \nabla \cdot \mathbf{F} = 0$$
$$\mathbf{F} = \mathbf{v}c \qquad \mathbf{v} = \begin{pmatrix} 1 \\ 0 \end{pmatrix} \tag{51}$$

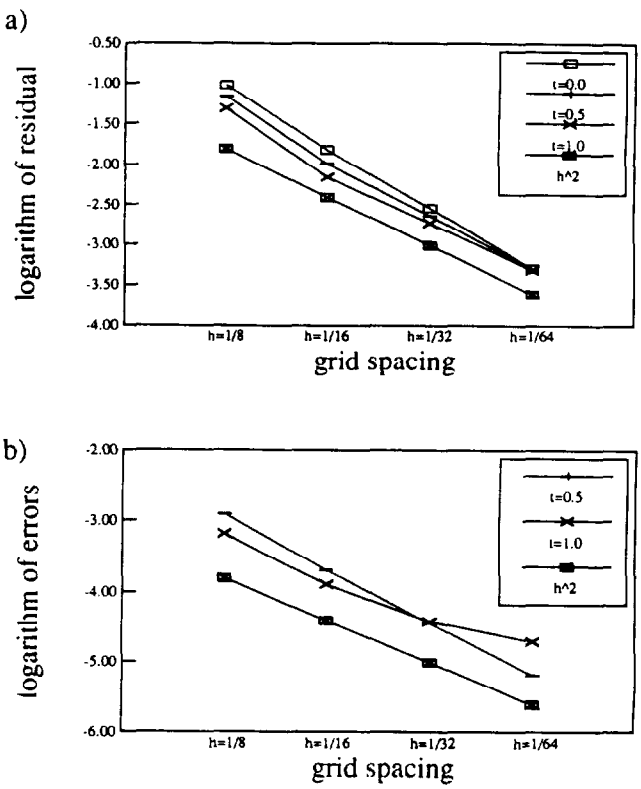

Fig. 10. Purely diffusive example. Logarithm of the norms of (*a*) the residuals and (*b*) solution errors plotted versus grid spacing.

TABLE 1. Parameters Used in the Solution of the One-Dimensional Convection-Diffusion Equation

Case	v, m/s	D, m^2/s	Δx, m	Pe
1	1.0	10.0	5.0	0.5
2	1.0	0.05	2.5	50
3	1.0	0.05	5.0	100
4	1.0	5×10^{-5}	5.0	10,000

Periodic boundary conditions are employed so that the effects of the boundaries do not influence the behavior of the numerical scheme. The following two different initial conditions are considered: a smooth sine square wave and a discontinuous square wave traveling with unitary velocity. The analytical solution is represented by a wave traveling throughout the domain with unitary period and maintaining the shape of the initial data. Simulations are performed for CFL numbers ranging from 0.5 to 1. The results are shown in Figures 5 to 8.

The scheme performs satisfactorily for any of the CFL numbers tested. In general, small amounts of numerical viscosity are added. Theoretically, numerical viscosity is the largest when $CFL = 0.5$. This is verified numerically in Figure 5. The peak concentration, however, is very well described. When $CFL = 0.9$ (Figure 6) artificial diffusion is noted only in the case of discontinuous initial data. A very good agreement with the analytical solution is obtained for the smooth sine square wave. At $CFL = 1$, exact results are obtained (Figure 7). The asymmetry of the concentration fronts for $CFL \neq 1$ stems from the particular limiter adopted in the formulation. It is interesting to note the well-known instability of the scheme when a first-order time discretization is used (Figure 8). Oscillations do not appear only because of the limiting process. These effects are especially evident in Figure 8a, where the sine square wave is completely squared after one period.

For the evaluation of the accuracy of the discretization of the dispersive fluxes, a pure diffusive equation with constant coefficients and Dirichlet boundary condition is solved. A Gaussian plume is used as the initial condition so that numerical and analytical solutions can easily be compared. Figure 9 shows the results of the simulations at different times.

For a better estimate of the convergence rate, Figure 10*a* reports the norms of the residuals plotted in logarithmic scale versus different grid spacings. The residual is defined as the difference between the differential space operator and the numerical space discretization operator, both of which act on the exact solution. It is therefore free of errors due to the temporal part at $t = 0$. Comparison with the h^2 line shows that the scheme is accurate to the second order. This is also verified by the analogous plot in Figure 10*b*, where the norm of the residuals is replaced by the norm of the solution errors (difference between numerical and analytical solutions). Only at a later time is a departure from the $O(h^2)$ behavior visible. This may be caused in part by accumulation errors due to time stepping.

The last one-dimensional example is a convection-diffusion problem with Dirichlet boundary conditions and zero initial condition, solved for different values of the cell-Peclet number. The parameters used in the simulation are reported in Table 1. The characteristic behavior displayed in the previous examples can be noticed. When the Peclet number is small, the numerical solutions agree well with the analytical solutions, (Figure 11*a*). At larger Peclet numbers, some numerical viscosity starts to appear, and the asymmetry caused by the limiting process is evident (Figures 11*b* and 11*c*). The concentration fronts are, however, well described, especially at high Peclet numbers (Figure 11*d*).

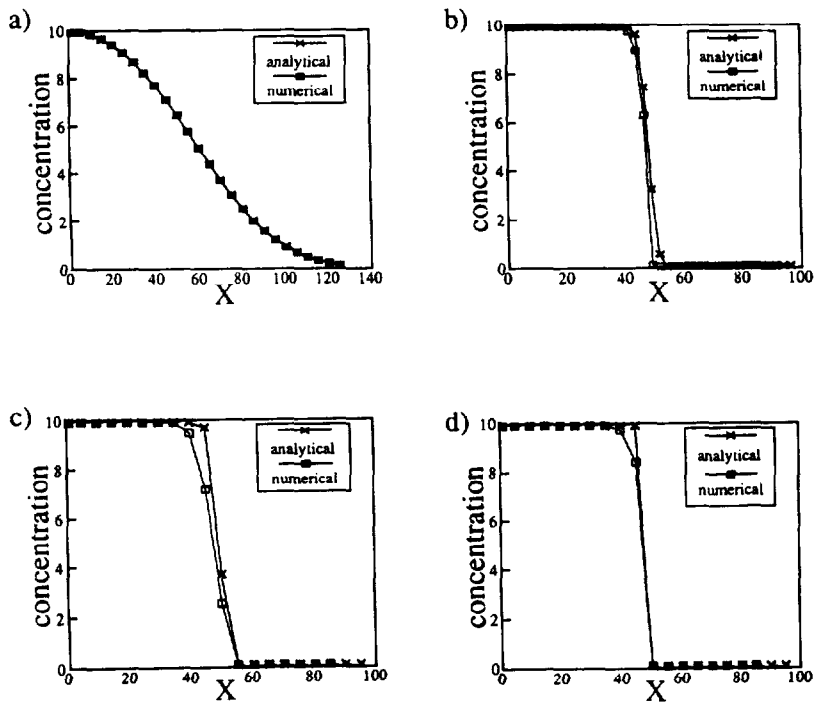

Fig. 11. Advection-diffusion example. Numerical versus analytical concentration for (*a*) $Pe = 0.5$, (*b*) $Pe = 50$, (*c*) $Pe = 100$, (*d*) $Pe = 10{,}000$.

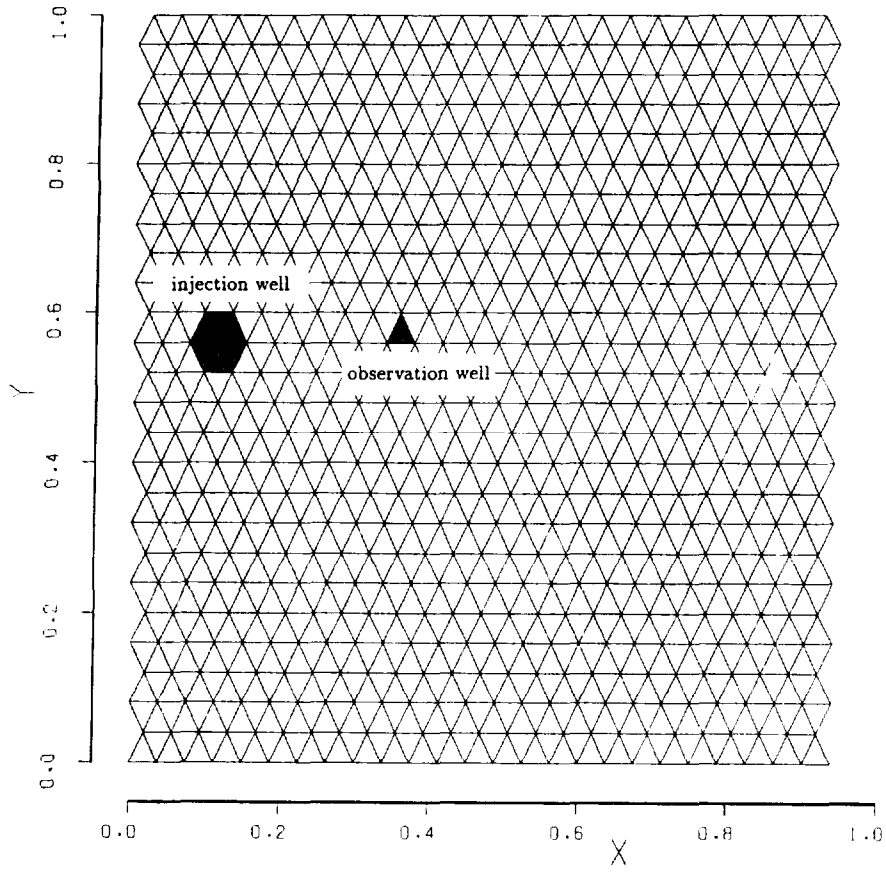

Fig. 12. Two-dimensional triangulation used in the solution of advection-dispersion-reaction equation; $\Delta y = 1/25$; $\Delta x = \Delta y \cos 15°$.

Two-Dimensional Simulations

To show the applicability of the proposed scheme to the solution of groundwater transport problems, the two-dimensional transport-reaction equations are solved on a square grid system. The hypothetical problem considered here is the prediction of the movement of a contaminant injected in an aquifer from a point source. A regional flow pattern is given and it is assumed not affected by the injection. The mathematical model can be stated as

$$\frac{\partial c}{\partial t} + \mathbf{v} \cdot \nabla c = \nabla \cdot \mathbf{D} \nabla c + \lambda(c^* - c) + R \qquad (52)$$

subject to the appropriate initial and boundary conditions. R is the source term representing the point injection, and $\lambda(c^* - c)$ represents the sorption reaction between the contaminant in the fluid phase and in the solid phase. It is assumed that the equilibrium concentration c^* is constant. This may not be a realistic assumption in the description of a physical process, since the equilibrium concentration is usually a function of the fluid phase concentration. It is, nonetheless, employed for this example problem so that the effects of the forcing functions can be isolated.

The regional flow is assumed to be along the x axis. All the parameters are considered constant and are appropriately scaled. The efficiency and accuracy of the scheme will not be affected by time or space-dependent coefficients as long as their variation is smooth, as is usually the case in groundwater problems.

The flow domain is discretized using 1225 equilateral triangles and is shown in Figure 12. The injection location and the observation well used to monitor the concentration are displayed. Injection starts at $t = 0$ and is turned off at $t = 0.5$. The concentration profiles over the whole domain are obtained at $t = 0.5$ and $t = 1$ or $t = 1.5$, and breakthrough curves at the observation well are also calculated. The parameters used for these simulations are summarized in Table 2.

Case 1: Dispersion and advection without reaction terms. The example is a convection-diffusion problem without reaction terms. The parameters are chosen so that a Peclet number of about 10 is used. From the level curves, shown in Figures 13*a* and 13*b*, dispersion along the y axis is clearly evident. The plume at $t = 1$ is more dispersed in any direction than the same plume at $t = 0.5$. The peak concentration has moved downstream and has decreased. The breakthrough curve, Figure 13*c*, also displays a pattern characteristic of these problems.

TABLE 2. Parameters Used in the Solution of the Two-Dimensional Convection-Dispersion-Reaction Equation

Case	D	λ	c^*
1	0.01	0.0	0.0
2	0.0	0.0	0.0
3	0.0	0.02	2.0
4	0.01	0.02	2.0

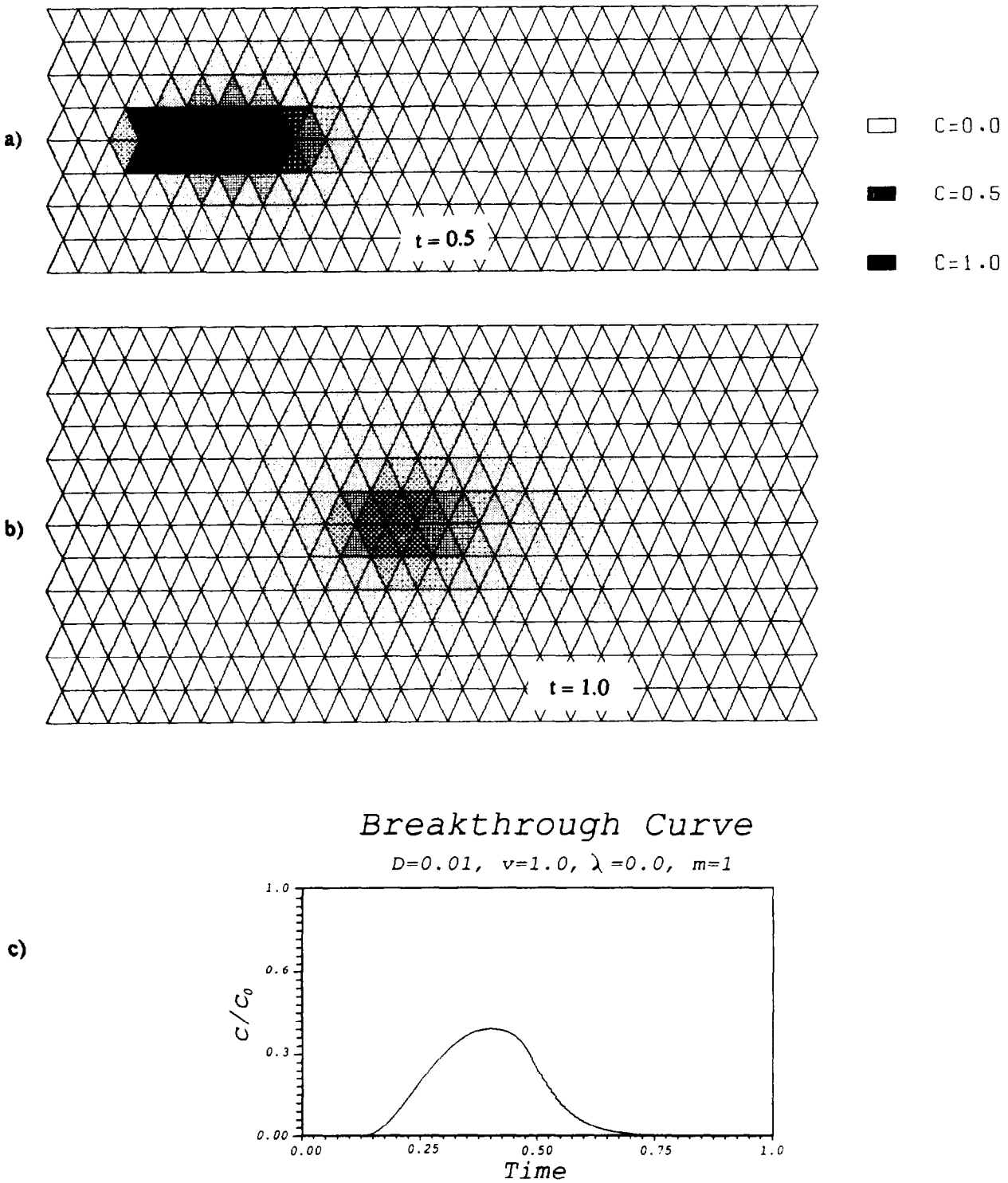

Fig. 13. Case 1. Dispersion and advection without reaction terms for (*a*) $t = 1.0$, (*b*) $t = 1.0$, and (*c*) breakthrough curve.

Case 2: Pure advection without reaction terms. In this example, a pure advective problem is considered. This is useful to check if the behavior of the numerical solution is consistent with the one-dimensional simulations. Again, small nonsymmetric numerical viscosity is visible in the concentration profiles (Figures 14*a* and 14*b*) along the x direction. No numerical viscosity can be seen along the y axis because this is a direction perpendicular to the regional flow, and the grid is oriented along this direction.

It is interesting to examine the breakthrough curve (Figure 14*c*). The observation well starts to detect the contaminant at $t \approx 0.2$, and then the concentration increases exponentially to reach its maximum at $t = 0.5$. This is the time at which the injection is turned off and the concentration

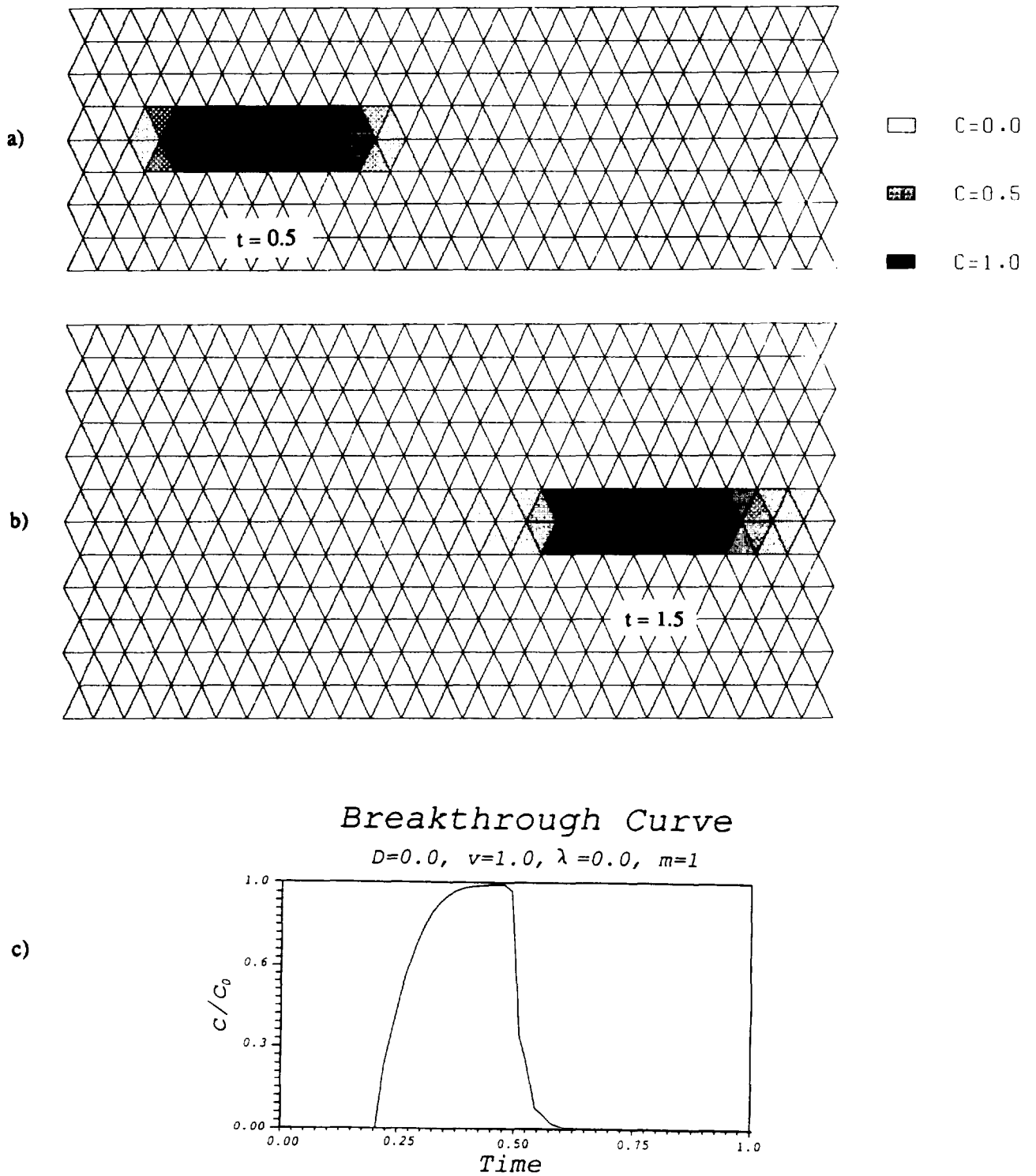

Fig. 14. Case 2. Pure advection without reaction terms for (*a*) $t = 0.5$, (*b*) $t = 1.5$, and (*c*) breakthrough curve.

achieves its maximum value at the injection well. It can be concluded that the peak concentration is not affected by numerical viscosity. The latter is visible on the right front of the breakthrough curve and it displays the characteristic behavior shown in the one-dimensional examples.

Cases 3 and 4: Pure advection and advection-dispersion with reaction terms. The behavior of the numerical scheme in the presence of reaction terms is analyzed. Equation (52) is solved by setting $\lambda = 0.2$. To better simulate a practical situation, the equilibrium concentration c^* is considered zero whenever the fluid phase concentration c is zero. It is set to a constant value whenever $c \neq 0$. Figures 15 and 16 show the results for advection-reaction and advection-dispersion-reaction problems.

The most visible effect due to the reaction terms is the appearance of a "tail" in the concentration profiles. The phenomenon is similar to a continuous injection at constant rate λc^*, which reaches a local steady state after the passage

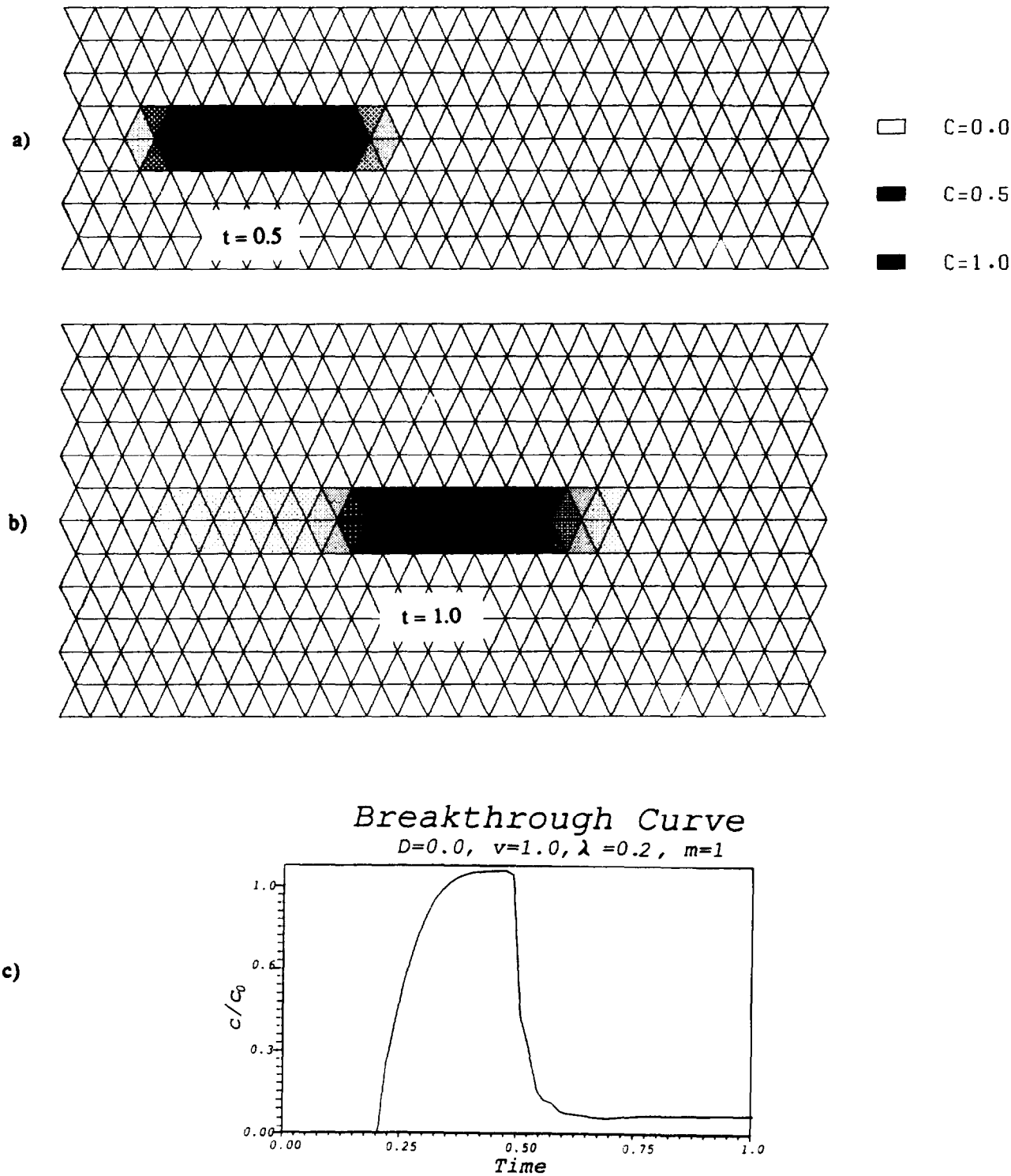

Fig. 15. Case 3. Pure advection with reaction terms for (*a*) $t = 0.5$, (*b*) $t = 1.0$, and (*c*) breakthrough curve.

of the plume (Figures 15*c* and 16*c*). In the pure advective case, the effect is visible only along the direction of the flow (Figure 15*b*). In the advective-dispersive case the "tail" is evident also in a direction orthogonal to the flow, because the dispersive fluxes are affected by this kind of reaction (Figure 16*b*). In a nonhypothetical scenario, where c^* is dependent on c, the tailing effect will be more pronounced and will not achieve steady state, but will vary with time until the contaminant is entirely or almost entirely removed from the solid phase.

Conclusions and Future Research

The following conclusions are worth emphasizing:

1. A finite volume approach based on triangular control elements is presented for the numerical solution of the

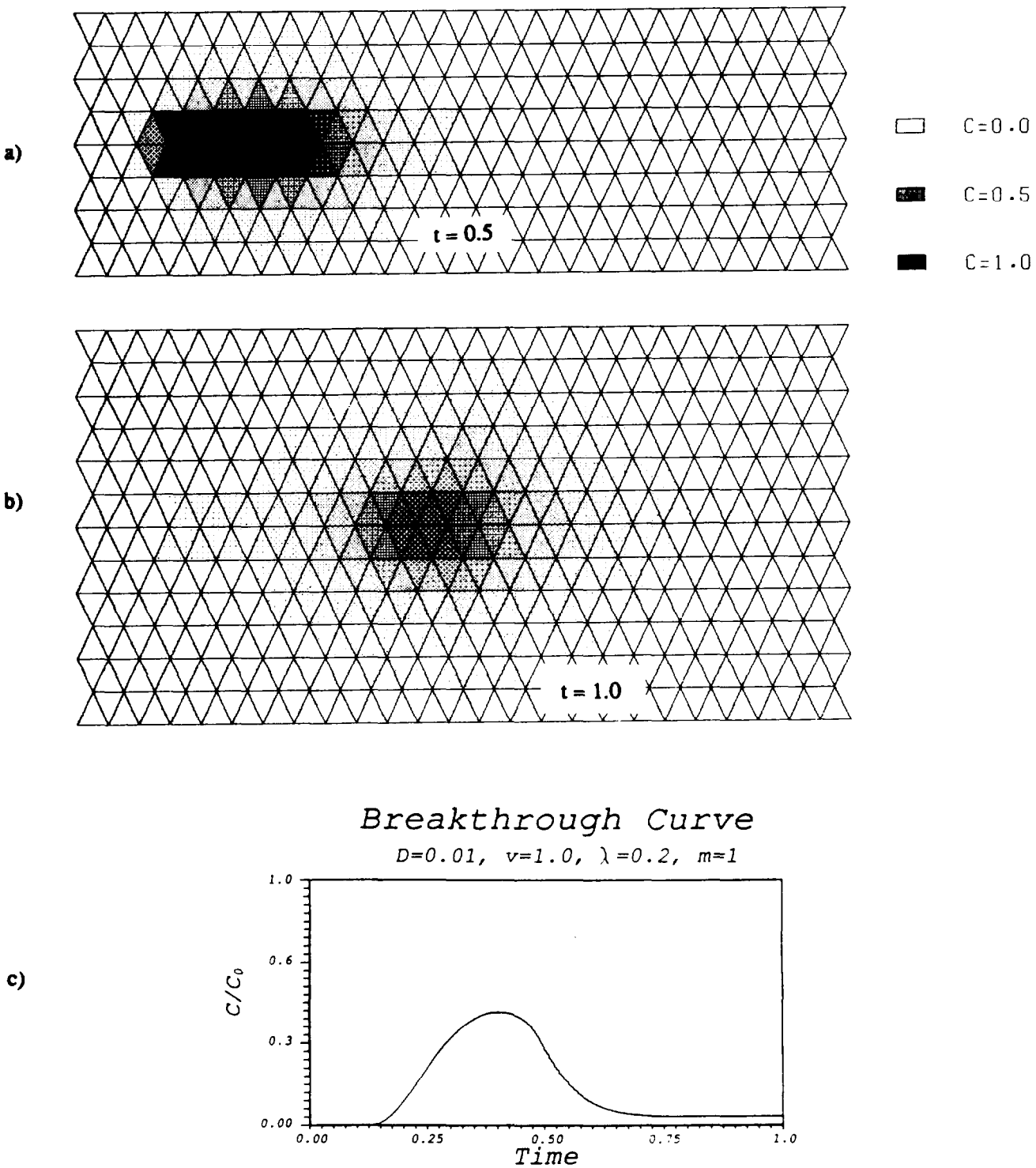

Fig. 16. Case 4. Dispersion and advection with reaction terms for (*a*) $t = 0.5$, (*b*) $t = 1.0$, and (*c*) breakthrough curve.

transport equation in groundwater contamination problems. By defining triangular cells, the scheme is flexible in handling geometrically complex domains and boundary conditions.

2. The formulation implements high-resolution upwind schemes for the discretization of the convective fluxes. These techniques, based on Godunov's method, allow accurate description of steep fronts with introduction of first-order numerical viscosity only in a neighborhood of the sharp front and are globally second-order accurate. As shown in the numerical examples, the scheme displays no spurious oscillations confirming the theoretical result that the formulation is TVNI. Analytical considerations, supported also by numerical experiments, suggest that the scheme remains second-order accurate for a full range of Peclet numbers. The reliability and flexibility of the proposed technique have been demonstrated by two-dimen-

sional example problem. Solutions obtained employing nonequilibrium reaction terms closely resemble concentration profiles obtained in field experiments.

3. The method possesses desirable properties that make the scheme very attractive especially for the solution of nonlinear problems. Its full capability may be best exploited for example in the area of multiphase flow and transport, where nonlinearities and coupling play an important role. The scheme is in fact particularly suited for nonlinear convective fluxes and may be extended for the discretization of systems of equations.

4. A more thorough examination of the accuracy of the scheme for nonequilateral triangles may be a subject of future research. As already mentioned, the technique will remain second-order accurate if the transition from element to element is smooth, and the distance of the centroid of each cell from the side varies always within the range of the truncation error $O(\Delta x^2)$. Therefore, shapes that are particularly narrow will destroy the global accuracy. Research along these direction is needed to ascertain the real accuracy of the method in all situations and to derive extensions to triangles of any shape. Another issue that should be addressed is the use of different limiting functions. Their role is in fact crucial for the description of steep fronts without incurring spurious oscillations. A limiter should be used to add numerical diffusion only when the latter is really necessary to maintain the TVNI property. In the literature several one-dimensional limiters have been presented that are able to accurately describe very steep fronts and discontinuities. However their extension to two spatial dimensions must be carefully studied in order to obtain two-dimensional limiters with the same characteristics.

Acknowledgments. The work of M.P. and W.W.-G.Y. was supported by the Toxic Substances Research and Teaching Program, University of California, Davis. The work of W.A.M. was supported by National Science Foundation grant DMS 88-11863 and office at Naval Research grant N00014-86-K-0691. The authors would like to thank the three anonymous reviewers for their constructive comments and suggestions.

REFERENCES

Bear, J., *Hydraulics of Groundwater*, McGraw-Hill, New York, 1979.

Chakravarthy, S., and S. Osher, Computing with high resolution: Upwind schemes for hyperbolic equations, *Lect. Notes Appl. Math.*, *22*, 57–86, 1985.

Farmer, C. L., Moving point techniques, paper presented at NATO Advanced Study Institute on Fundamentals of Transport Phenomena in Porous Media, Newark, Del., July 14–23, 1985.

Godunov, S. K., Finite difference method for numerical computation of discontinuous solution of the equations of fluid dynamics, *Math. Sb.*, *47*(3), 271–306, 1959.

Goodman, J. B., and R. J. LeVeque, A geometric approach to high resolution TVD schemes, *SIAM J. Numer. Anal.*, *25*(2), 268–284, 1988.

Harten, A., High resolution schemes for hyperbolic conservation laws, *J. Comput. Phys.*, *49*, 357–393, 1983.

Neuman, S. P., A Eulerian-Lagrangian numerical scheme for the dispersion-convection equation using conjugate space-time grids, *J. Comput. Phys.*, *41*, 270–294, 1981.

Neuman, S. P., Adaptive Eulerian-Lagrangian finite element method for advection-dispersion, *Int. J. Numer. Methods Eng.*, *20*, 321–337, 1984.

Peyret, R., and T. D. Taylor, *Computational Methods for Fluid Flow*, Springer-Verlag, New York, 1983.

Putti, M., A triangular finite volume approach for the solution of the contaminant transport equations in groundwater, Ph.D. dissertation, *Dep. of Civ. Eng., Univ. of Calif., Los Angeles, 1989.*

Richtmeyer, R. D., and K. W. Morton, *Difference Methods for Initial-Value Problems*, Wiley-Interscience, New York, 1967.

Roe, P. L., Characteristic-based schemes for the Euler equation, *Annu. Rev. Fluid Mech.*, *18*, 337–365, 1986.

Sun, N.-Z., and W. W.-G. Yeh, A proposed upstream weight numerical method for simulating pollutant transport in groundwater, *Water Resour. Res.*, *19*(6), 1489–1500, 1983.

Sweby, P. K., High resolution schemes using flux limiters for hyperbolic conservation laws, *SIAM J. Numer. Anal.*, *21*(5), 995–1011, 1984.

Sweby, P. K., High resolution TVD schemes using flux limiters, *Lect. Notes Appl Math.*, *22*, 289–309, 1985.

van Albada, G. D., B. Van Leer, and W. W. Robers, Jr., A comparative study of computational methods in cosmic gas dynamics, *Astron. Astrophys.*, *108*, 76–86, 1982.

van Leer, B., Towards the ultimate conservative finite difference scheme, III, Upstream centered finite difference schemes for ideal compressible flow, *J. Comput. Phys.*, *23*, 263–275, 1977*a*.

van Leer, B., Towards the ultimate conservative finite difference scheme, IV, A new approach to numerical convection, *J. Comput. Phys.*, *23*, 276–299, 1977*b*.

van Leer, B., Upwind-difference methods for aerodynamic problems governed by the Euler equations, *Lect. Notes Appl. Math.*, *22*, 327–336, 1985.

Zienkiewicz, D. C., *The Finite Element Method*, McGraw-Hill, New York, 1986.

W. A. Mulder, Koninklijke/Shell Exploratie en Produktie Laboratorium, Postbus 60, 2280 AB Rijswijk, The Netherlands.

M. Putti and W. W.-G. Yeh, Department of Civil Engineering, University of California, Los Angeles, 405 Hilgard Avenue, Los Angeles, CA 90024.

(Received August 29, 1989;
revised July 25, 1990;
accepted August 7, 1990.)